NONTHERMAL RADIO EMISSIONS FROM URANUS

W. M. Farrell*

Abstract

Uranus is a very complex radio source, possessing at least 8 nonthermal radio components, including three temporal bursty emissions, many smooth emissions, and lightning–like sferic signals. The most powerful of these emissions are generated at and beamed into the nightside hemisphere at nearly 10^7 W. In this paper, a review of the past and current research of the Uranian radio emissions is presented. Extra emphasis will be placed on new studies performed since the last Radio Emissions from Planetary Magnetospheres workshop held in 1987.

1 Introduction

In January of 1986, the Voyager–2 spacecraft made an historic encounter with the seventh planet in our solar system, Uranus. During the encounter, it became evident that the planet is an active generator of nonthermal radio emissions, making it the fourth known 'radio' planet in the solar system. Since the encounter, over 40 studies of the emissions have been performed, and these will now be highlighted here.

Of the eleven experiments onboard Voyager, two are radio instruments specifically designed to detect radio and plasma wave emissions originating within planetary magnetospheres. One of these instruments is the Planetary Radio Astronomy (PRA) experiment, which consists of a receiver having 200 discrete frequency channels operating between 1.2 kHz and 40 MHz. The receiver samples signals from two orthogonal monopole antennas of 10–meter length. In normal operation, all 200 channels are sequentially sampled every 6 seconds. In other operational modes, high temporal resolution data can be obtained from fixed channels. Using hybrid discriminator circuitry, the receiver can make measurements of emission polarization sense (i.e., left–handed (LH) and right–handed (RH)) in the spacecraft frame of reference) which is a valuable tool for identification and localization of various radio components. For further information, a full description of this instrument can be found in Warwick et al. [1977]. The other radio instrument onboard

*Planetary Magnetospheres Branch, Laboratory for Extraterrestrial Physics, NASA/Goddard Space light Center, Greenbelt, MD 20771

Voyager is the Plasma Wave (PWS) experiment, whose components include a 16–channel spectrum analyzer that operates between 10 Hz and 56.2 kHz, sampling from the same antenna system used by the PRA (but in a dipole configuration). In normal operation, all 16 channels are sampled every 4 seconds. Besides the spectrum analyzer, the PWS experiment has a wideband waveform receiver that samples the voltage as a function of time in a 50 Hz–12 kHz frequency regime. Measurements are obtained at the Nyquist frequency (28800 samples per second) and returned via the high rate telemetry stream used by the imager. For further information on these receivers of PWS experiment, a complete description can be found in Scarf and Gurnett [1977].

Both the PRA and PWS experiments were extraordinarily successful during the previous encounters with Jupiter and Saturn, and investigators fully anticipated comparable success at Uranus. In particular, estimating the conversion of solar wind input power, Kennel and Maggs [1976] suggested that Uranus would be a strong emitter of nonthermal radio emission, possibly generating as much as 10^{10} W of radio power. Using the Imp–6 radio astronomy experiment, Brown [1976] identified a set of burst events suspected to be of Uranian origin. These events had a peak in frequency near 500 kHz, and their intensities suggested that the Uranian radio source emits about 10^{11} W of power. Based on a radiometric Bodes law, which functionally relates the radio power to solar wind input energy and planetary magnetic moment, Desch and Kaiser [1984] predicted that Uranus should emit about 10^7–10^8 W of radio power, as long as the planet possessed a magnetic moment greater than $0.1\ \Gamma\ R_U^3$. This predicted power was much less than that proposed by Kennel and Maggs [1976] and that inferred from the Brown [1976] observation. Based on the radiometric Bodes law, Desch and Kaiser [1984] suggested that Uranus would become detectable by the PRA receiver about nine months before encounter, when the spacecraft was about 2.5 AU from the planet. Observational evidence of an active Uranian magnetosphere was provided by IUE observations of enhanced Lyman–α flux from Uranus [Clarke, 1982]. These UV emissions were suspected to originate from the auroral region. In general, such auroral active sites are also known to generate strong radio emission. Hence, these pre–encounter studies all suggested that Uranus was an active emitter of relatively strong nonthermal radio waves, and such waves were expected to be detected by the Voyager PRA at least nine months before the planetary encounter, by May 1985.

Unfortunately, during most of the year before encounter, no Uranian radio emissions were detected. Even as late as November of 1985, seven months after the predicted time of discovery, no emissions had been observed. This lack of detection was quite disconcerting to the PRA and PWS investigators. A number of possible scenarios were presented to

Figure 1: (color plot, next page) A color dynamic spectrum of the PRA measurements during a six day period near the Uranus encounter. Closest approach to the planet occurred near 1800 SCET on 24 January. Note that prior to closest approach, radio activity was limited to relatively low frequencies but, thereafter, became intense and broadbanded with both a bursty and smooth emission extending up to nearly 800 kHz (Figure originally appeared in Farrell and Calvert, [1989a]).

explain this lack of detection. Curtis [1985] suggested that Uranus' dominate cyclotron emissions, those presumably like Earth's AKR, and Jupiter's DAM, are generated on the planet's nightside and thus are beamed away from the incoming spacecraft. This prediction was based upon the hypothesis that the nightside auroral zone is relatively devoid of plasma, and thus is the best location for the development of the X–mode cyclotron resonance instability. Hill and Dessler [1985] suggested that the Uranian radio emissions are inherently weak because planetary spin processes are driving the magnetosphere, rather than solar wind processes as assumed by Desch and Kaiser [1984]. Consequently, the spin–driven radio emissions were predicted to be initially detected about four months before closest approach, in September 1985. Of course, the worst possible scenario to explain the lack of radio wave detection was if the planet, itself, possessed a very weak magnetic field, thereby failing to generate cyclotron emission. If this scenario proved to be true, from a radio astronomy perspective, Uranus would be relatively uninteresting.

In fact, the discovery of radio emission from Uranus was made about five days before closest approach using the PWS experiment; these new events being narrowbanded radio bursts detected at around 50 kHz [Gurnett et al., 1986]. About a day later, a narrowband smooth component was first identified in the PRA measurements [Warwick et al., 1986]. However, Uranian radio emissions became quite intense after closest approach, when Voyager was outbound and over the nightside auroral region. During the outbound period, two very strong, broadbanded radio components continually reappeared as Voyager receded from the planet. Figure 1 is a Voyager–2 PRA color dynamic spectrum showing the observations during the Uranus encounter. Closest approach to the planet occurred at 1759 SCET on 24 January. Note that prior to closest approach, while Voyager was inbound, most of the radio activity was observed below about 100 kHz (the narrowbanded activity near 350 kHz between 0000–0500 SCET on 24 January is spacecraft–related noise). However, once Voyager crossed the magnetic equator (1320 SCET on 24 January) and came in view of the nightside magnetic pole, significant broadband radio activity was seen with frequencies as high as 800 kHz. All totaled, both the PRA and PWS experiments detected at least 7 new nonthermal radio components at Uranus. Also, near closest approach, lightning–generated sferics were observed in the PRA experiment [Zarka and Pedersen, 1986]. Consequently, Uranus proved to be a more complex radio emitter than initially suspected.

In retrospect, the most probable reason for the day/night radio emission asymmetry at Uranus is the unusual orientation and position of the planetary magnetic dipole. As described by Ness et al. [1986], the Offset–Tilted–Dipole model possesses a dipole axis orientation tilted 60° from the rotation axis, and a dipole center shifted 0.3 R_U southward from the planet center. Due to the large offset, the magnetic field strength near the south magnetic polar region is far stronger than that in the northern regions. Consequently, there is a larger spatial region above the south magnetic pole where $f_{pe}/f_{ce} < 1$ and thus a larger wave growth region where X–mode wave generation is favored. The Q3 field model [Connerney et al., 1987] that includes internal sources indicates that the field near the planet surface is very complex, particularly near the weaker, north magnetic polar region.

2 Uranus as a radio source: Specific components

The Uranian magnetosphere and atmosphere is the source of at least 8 different radio emissions, each having quite different temporal and spectral structures from one another. Table 1 lists the major components and their characteristics. The emissions can basically

Table 1: The Major Uranian Radio Components

Component	**Freq. (kHz)**	**Polar.**	**Mode**	**Presumed Source**[3]	**# of Studies**
n–bursts	16–117	RH	R–X	near NMP[4]	8
n–smooth[1]	20–350	LH/RH	R–X	mag. equat.	9
O–mode	100–300	LH	L–O	Near NMP	2
Continuum	1–3,>7	?	?	mag. equat.	1
5 kHz Bursty	3–10	?	?	Miranda L–shell	2
b–smooth[2]	150–900	LH	R–X	near SMP[5]	18
b–bursty	200–800	LH	R–X	near SMP	8
UED	0.9–40 MHz	UN	UN	Atmosphere	1

[1] Also called 'SLF'
[2] Also called 'SHF'
[3] See text for details
[4] NMP: North Magnetic Pole
[5] SMP: South Magnetic Pole

be divided into two groups based upon their temporal duration. The first group are the 'smooth' or 'continuous' emissions, so named because their temporal duration is many hours. The second group are the 'bursty' emissions, so named because their temporal duration is relatively short (< 10 minutes). Bursty emissions have been observed at other planets (i.e., Jovian S–bursts), but Uranus possessed at least three such components. Clearly, the abundance of this emission type suggests the presence of some impulsive or bursty physical phenomena (or phenomenon) which has yet to be suitably identified on a global scale.

2.1 Narrowbanded Radio Bursts

This emission, called n–bursty for short, was the first detected from Uranus, and was the first indication that the planet possessed a significant magnetic field [Gurnett et al., 1986]. N–burst events were first detected on 19 January 1986, about 5 days prior to Voyager's closest approach (CA) to the planet, in the 31.1 and 56.2 kHz channels of the PWS receiver [Gurnett et al., 1986]. However, careful reexamination of the PRA data revealed the presence of n–bursts as far back as 15 December 1985, nearly 35 days before CA [Desch et al., 1989]. Because they strongly resemble single–channel noise spikes, the events simply went unnoticed until the discovery day.

A comprehensive analysis of all n–burst events detected in both the PWS and PRA receivers was performed by Desch et al. [1989]. It was concluded that n–burst activity extended in frequency from 17 to 116 kHz, with the intrinsic bandwidth of an individual burst event being about 5 kHz. Consequently, the ratio of bandwidth–to–center frequency $\Delta f/f$ is on the order of 0.1 for this particular emission, indicating a relatively narrowbanded signal.

Close to the planet, burst events at a particular frequency tended to be clustered into groups. However, statistical analysis using high–resolution PRA data suggest individual burst events possess a nominal temporal duration of about 250 milliseconds [Desch et al., 1989]. Figure 2, originally from Desch et al. [1989], displays the PRA measurements on 24 January 1986 with progressively improving temporal resolutions. In panel (a), 48–second temporal averaged samples are presented which clearly shows a cluster of n–burst events between 0716 and 0800 SCET. Panel (b) shows the same measurements with 6–second resolution. Note that there is partial resolution of individual 'bursts' within the cluster at this resolution. Panel (c) shows a subsection of (b) with 60 millisecond sampling. Individual bursts are now fully resolved; these possessing a temporal duration on the order of hundreds of milliseconds.

While Voyager was inbound, burst events were observed at all longitudes. However, burst activity was greatly enhanced when the north magnetic pole of the planet tipped towards the spacecraft (i.e., when Voyager was at high northern magnetic latitudes) [Desch et al., 1989]. The n–burst activity also ceased after CA, when Voyager was out of view of the north magnetic pole. Besides a correlation with magnetic latitude, the long–termed burst activity was found to be correlated with the solar wind density at Uranus [Desch et al., 1989], which suggests an external control of this emission similar to the Saturnian kilometric [Desch and Rucker, 1983] and Jovian hectometric [Zarka and Genova, 1983; Desch and Barrow, 1984] emissions.

Since the burst activity increases with increasing north magnetic latitude, Desch et al. [1989] suggested that the n–burst radio source lies very near the north magnetic pole of the planet, possibly on the same active field lines associated with the dayside O–mode emission (see below). Also, for a source in the northern magnetic hemisphere, the observed polarization of the bursts (RH) is consistent with X–mode radiation [Desch et al., 1989]. By examining the n–burst beaming at high and low frequencies, Farrell et al. [1990a] concluded that the narrowbanded burst radio source is located near the north magnetic pole, on field lines of Q3 [Connerney et al., 1987] L–shell of 4 to 11 that extend into the

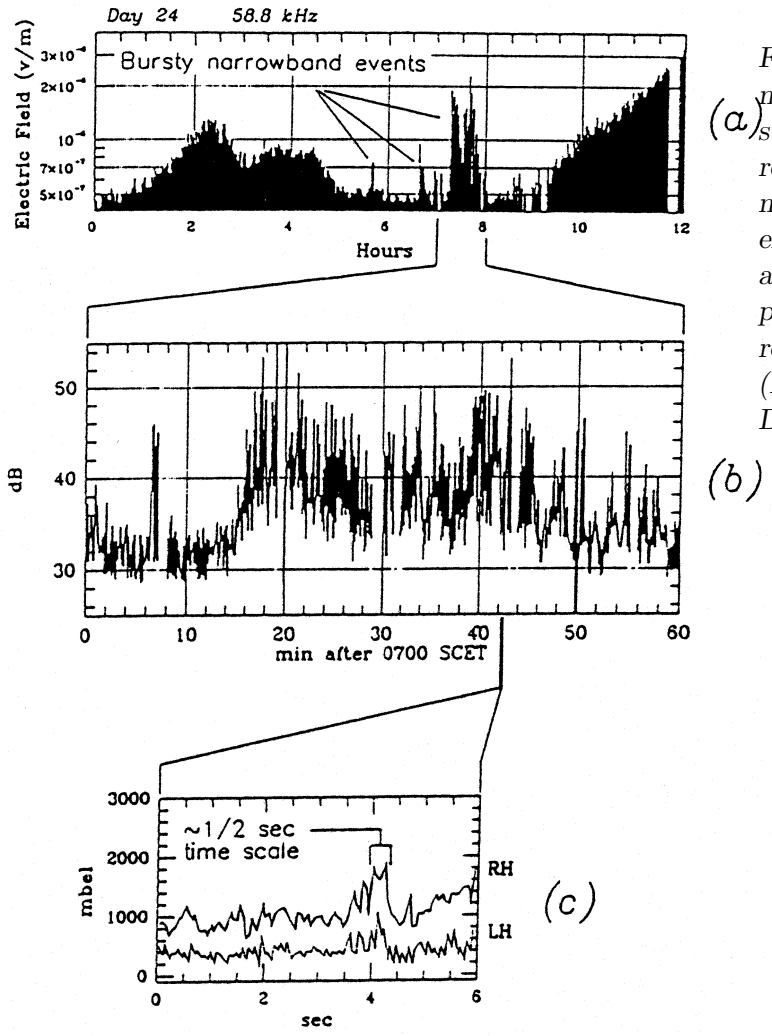

Figure 2: Voyager PRA measurements of an n–burst episode with successively improving temporal resolution. In (a), the measurements are 48–second temporal averages, in (b), 6–second samples, and in (c) 60 millisecond samples. Individual burst events are resolved at the highest resolution. (Figure originally appeared in Desch et al. [1989].)

dayside. Confirmation of such a dayside location has been made by Curran and Menietti [1990] using ray tracing arguments. The proposed location lies near the boundary between open and closed field lines, and thus is suspected to lie at the low latitude edge of the northern polar cusp/cleft region. The correlation of burst activity with solar wind density would certainly be consistent with a cusp source, since solar wind particles can directly enter the magnetosphere at this point, thereby affecting the generation of the radio signals.

One possible generation mechanism of the X–mode n–bursts at Uranus is the cyclotron resonance process originally described by Wu and Lee [1979]. However, a recent adaptation of this process has been presented by Wong and Goldstein [1990], who modeled the cyclotron emission process using a beam–dominate electron distribution, rather than a loss cone distribution, thereby obtaining intermediate values of wave normal angles more consistent with the bursts. To explain the bursty emission behavior, Farrell et al. [1992] have suggested that MHD surface waves created at the frontside magnetopause propagate to low altitudes within cusp, where they mode convert to kinetic Alfvén waves (KAWs) that drive the radio emission.

2.2 Narrowbanded Smooth Emission

The second component detected from Uranus was the narrowbanded smooth (n–smooth) emission first observed about 5 days prior to CA, and seen for at least the next 12 days throughout both the inbound and outbound encounter periods [Warwick et al., 1986; Leblanc et al., 1987; Kaiser et al., 1989]. The emission had a spectral peak near 60 kHz, with half–power points of about 20 kHz [Leblanc et al., 1987; Kaiser et al., 1989]. Consequently, $\Delta f/f < 0.5$, and the emission can be considered relatively narrowbanded (although not as narrowbanded as the n–bursts).

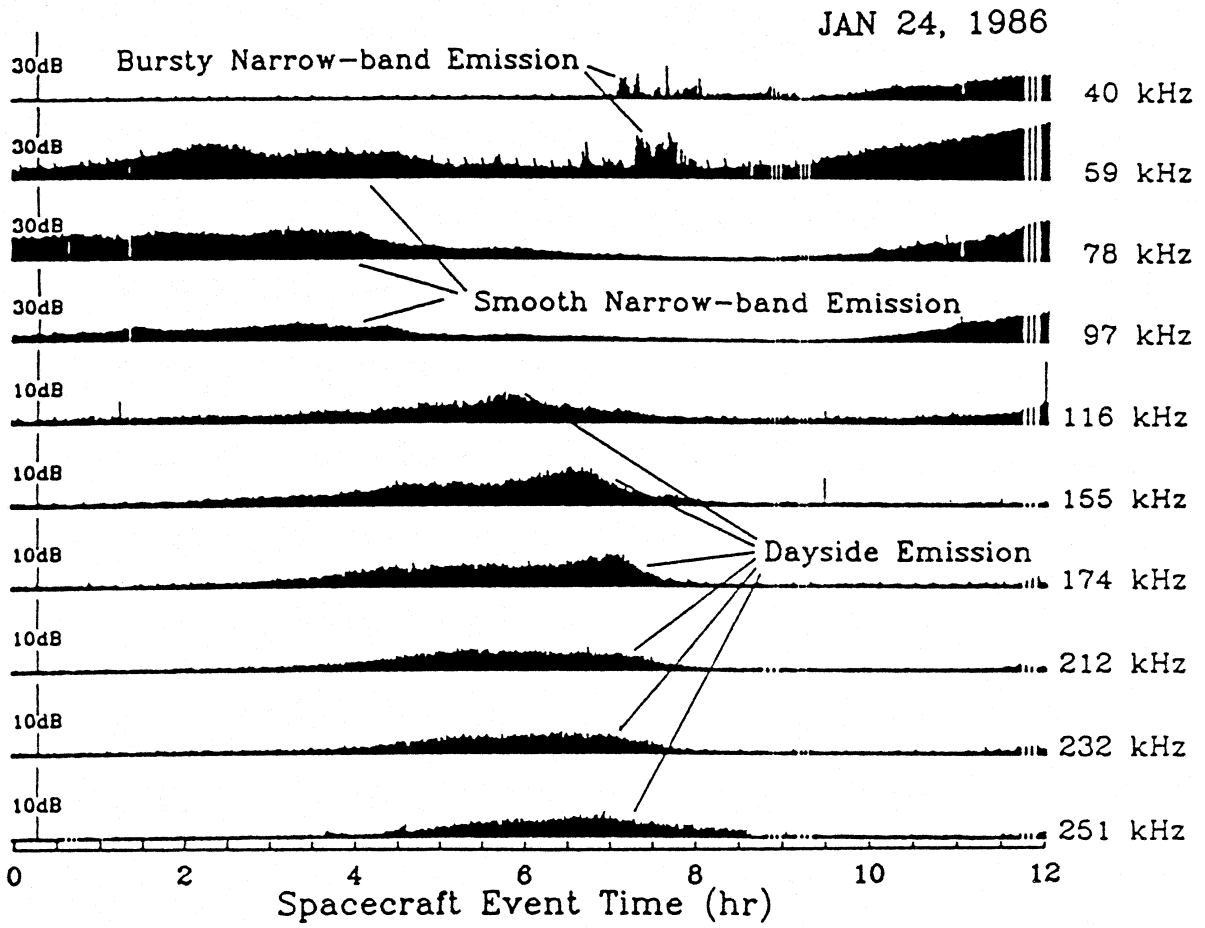

Figure 3: Voyager PRA measurements in 11 channels during a 12 hour period prior to closest approach when the n–bursty, n–smooth and dayside O–mode emission all appeared. (Figure originally appeared in Desch and Kaiser [1987]).

Figure 3, from Desch and Kaiser [1987], shows part of an n–smooth event occurring about 15 hours before closest approach. Clearly, the n–smooth emission is continuous over many hours and has a distinctly different character from the n–bursty signals which are also shown in the Figure. The n–smooth emission, as observed by Voyager, possessed three distinct features in its occurrence pattern: First, the emission amplitude varied as a function of rotational phase. Second, the polarization of the emission reversed from left to right handed as Voyager crossed the magnetic equator. Finally, the n–smooth intensity displayed a distinct reduction or 'dropout' of nearly 15 dB around closest approach.

The source localization of the n–smooth emission has been an evolving process, with studies initially attempting to fit either the intensity pattern or polarization signature described above, but not both features. Warwick et al. [1986] suggested that the n–smooth and broadband smooth (see below) emissions are one and the same emission, originating from the same source location. However, they suggest the dayside beamed emissions are limited to a narrow band at low frequencies due to the presence of an extended dayside plasmasphere which blocks out the high frequency component. Gulkis and Carr [1987] demonstrated that a single extended cyclotron emission source ($\sim 120^\circ$ in longitude) at relatively high L–shells (~ 33) possessing a relatively thick beam ($\sim 35^\circ$) could account for the occurrences of both the dayside/narrowbanded and nightside/broadbanded smooth emission. Both studies modeled the intensity pattern, but neither explained the observed polarization changes.

Examining the n–smooth intrinsic polarization reversal at the magnetic equator crossing, Leblanc et al. [1987] derived a radio source originating near the north magnetic pole, somewhere in the region between 10°N, 70°W to 40°N, 25°W. Lecacheux and Ortega–Molina [1987] further localized this source location to a relatively small region near 40°N, 25°W using the polarization reversals observed during spacecraft roll maneuvers. However, Kaiser et al. [1989] demonstrated that the north polar source derived by Lecacheux and Ortega–Molina [1987] should be occulted for about 5 hours by the Uranian ionosphere every rotation during the Voyager outbound period. Such a dramatic occultation signature was not seen in the PRA measurements, thus the proposed north polar source became questionable.

More recent studies attempted to fit all the major intensity and polarization features of the emission, which could be done best by sources at relatively low latitudes. Sawyer et al. [1991] demonstrated that two extended sources located at $\pm$ 20° magnetic latitude could account for both the intensity and polarization of the n–smooth emission. Kaiser et al. [1989] demonstrated that a cyclotron radio source extending around the magnetic equator could account for the major features of the emission intensity and polarization. They indicate that the most intense emission is associated with a source connected to the ϵ ring. This ring is believed to absorb small pitch–angled electrons, leaving an unstable ring–type electron distribution on connected drift shells. Also, the emission polarization as measured by the PRA is consistent with the X–mode, thereby ruling out the linear conversion process for equator–type emissions proposed by Jones [1976,1980]. Further study of this n–smooth location was performed by Menietti and Curran [1990a], who suggest, via ray tracing arguments, that the emission could be fundamental X–mode emission, and that conditions may also be favorable for the development of second harmonic emission. Very recently, Rabl et al. [1991, 1992] compared the high–latitude north magnetic and magnetic equator sources, and confirmed the latter as the better fitting source.

2.3 Dayside O–mode Emission

About 14 hours before closest approach, when Voyager was approximately 30 R_U from Uranus, a smooth–type emission was observed for approximately 4 continuous hours at frequencies between 116 and 350 kHz [Desch and Kaiser, 1987]. This emission appeared

very similar to the n–smooth emission observed during the inbound period at lower frequencies. However, based on emission frequency and polarization arguments, Desch and Kaiser [1987] explicitly demonstrate that this higher frequency dayside emission is distinctly different from the n–smooth emission detected below 100 kHz. Figure 3 shows the single occurrence of this higher frequency dayside emission, along with the n–smooth emission and a cluster of n–bursts.

The detection of this dayside component corresponded to a time when Voyager's angular displacement with respect to the north magnetic pole was a minimum (i.e., Voyager was at its highest northern magnetic latitude) [Desch and Kaiser, 1987]. This observation suggests a radio source located near the Uranian north magnetic pole. This inference was confirmed by examination of the radio horizon at emission commencement and cessation [Desch and Kaiser, 1987]. In particular, the radio source was found to lie in a region just southwest of the northern magnetic dipole tip, centered at about 0°N, 60°W. Further, this location is believed to be magnetically connected to the active region generating the broadband smooth emission in the nightside hemisphere. Thus, the set of active field lines associated with this dayside emission are presumably connecting two radio sources, each located in conjugate hemispheres.

Based upon the observed emission polarization, Desch and Kaiser [1987] conclude that the emission is propagating in the ordinary mode (O–mode). Further, using the electron density profile obtained by the Radio Science (RSS) experiment, they conclude that $f_{pe}/f_{ce} \sim 1$ near the radio source. Because of the relatively high plasma density, it is believed that the dayside O–mode emission is generated directly via a cyclotron resonance process, and is not a byproduct of some X–mode conversion process [Desch and Kaiser, 1987].

Recent confirmation of the O–mode radio source found by Desch and Kaiser [1987] was provided by Menietti and Curran [1990b] using ray tracing arguments. In their analysis, the actual source extent varied, depending on the particular density model used in their analysis.

2.4 Continuum Radiation

Like at Earth, Jupiter, and Saturn, Uranus possess a radio component known as continuum radiation [Gurnett et al., 1986; Kurth et al., 1990]. As described by Kurth et al. [1990], the most unique feature of this emission is not its signal strength, which is actually relatively weak, but the fact that the component is observed at each of the radio planets. Uranian continuum radiation is most easily seen in the PWS wideband receiver, having a flat spectrum between 1 and 3 kHz [Kurth et al., 1990]. Figure 4, from Kurth et al. [1990], is an electric field spectrum obtained from the PWS wideband receiver during a period when the continuum emission was observed. Note that the emission is prevalent in the spectra between 1 and 3 kHz. Clear identification of the emission could be made at the magnetopause crossing, where it abruptly appeared in both the PWS spectrum analyzer at 1.78 kHz and PRA receiver at 1.2 kHz. In the latter receiver, it persisted continuously for nearly 2 hours, appearing as right hand polarized emission in the spacecraft frame. This polarization is consistent with the proposed continuum radiation generation process by Jones [1976, 1980]. Based on the PWS and PRA observations, Kurth et al. [1990]

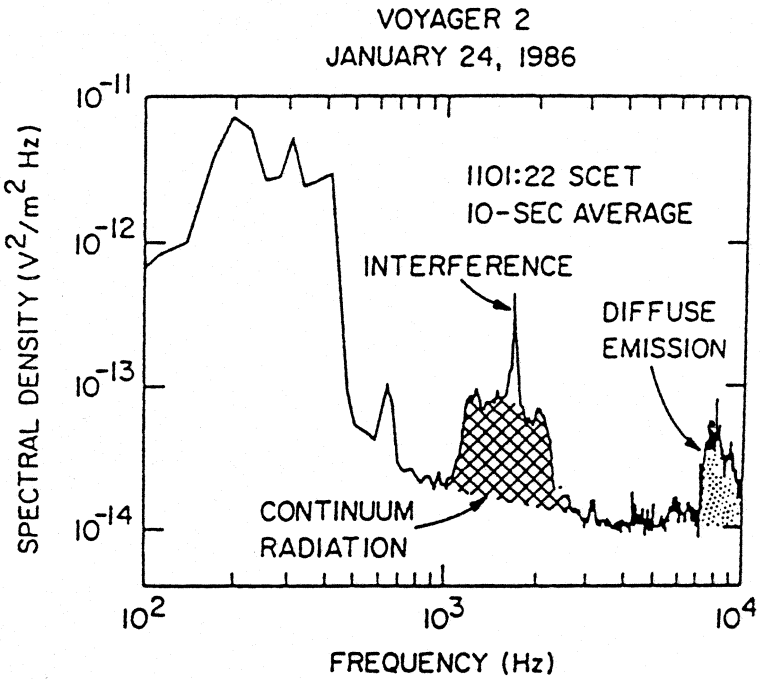

Figure 4: The electric field spectrum obtained from the PWS wideband experiment during a period when the continuum radiation was observed. Note that the diffuse emission is also present at frequencies greater than 7 kHz. (Figure originally appeared in Kurth et al. [1990].)

conclude that the emission is trapped in the magnetospheric density cavity between the magnetopause and the inner magnetosphere. Hence, its occurrence and polarization make it analogous to the continuum emission observed at Earth.

Besides the 1–3 kHz emission, the PWS wideband receiver also detected a diffuse emission at higher frequencies, typically greater than 6 kHz, which might also be a component of the continuum radiation [Kurth et al., 1990]. As discussed in Kurth et al. [1990], the exact interpretation of these diffuse bands is difficult without an AC magnetic sensor (i.e., a search coil). Figure 4 also shows the diffuse emission, observed above 7 kHz.

It is strongly suspected that the origin of the continuum emission is the linear conversion process proposed by Jones [1976, 1980]. In this process, electrostatic emissions (i.e., upper hybrid waves) convert to Z–mode emissions in a region possessing a plasma density gradient, and then propagate through a radio window at f_{pe} to become escaping O–mode emissions. As discussed in Kurth et al. [1990], intense electrostatic emissions were observed at the magnetic equator crossing, and these emissions are believed to be the driver of the escaping O–mode emission detected by Voyager.

2.5 5 kHz Radio Bursts

An emission observed exclusively by the PWS experiment was a very narrowbanded, bursty emission lying between 3–10 kHz. These bursts went undetected in the PRA receiver, since they lie in between the first (1.2 kHz) and second (19.6 kHz) PRA channels. The bulk of the burst observations were made during the outbound period, with the emission being seen possibly as far as 570 R_U from the planet. As described by Kurth et al. [1986], the narrowbanded nature of the emission makes it appear similar to escaping, nonthermal continuum radiation seen in other planetary magnetospheres; yet it is much

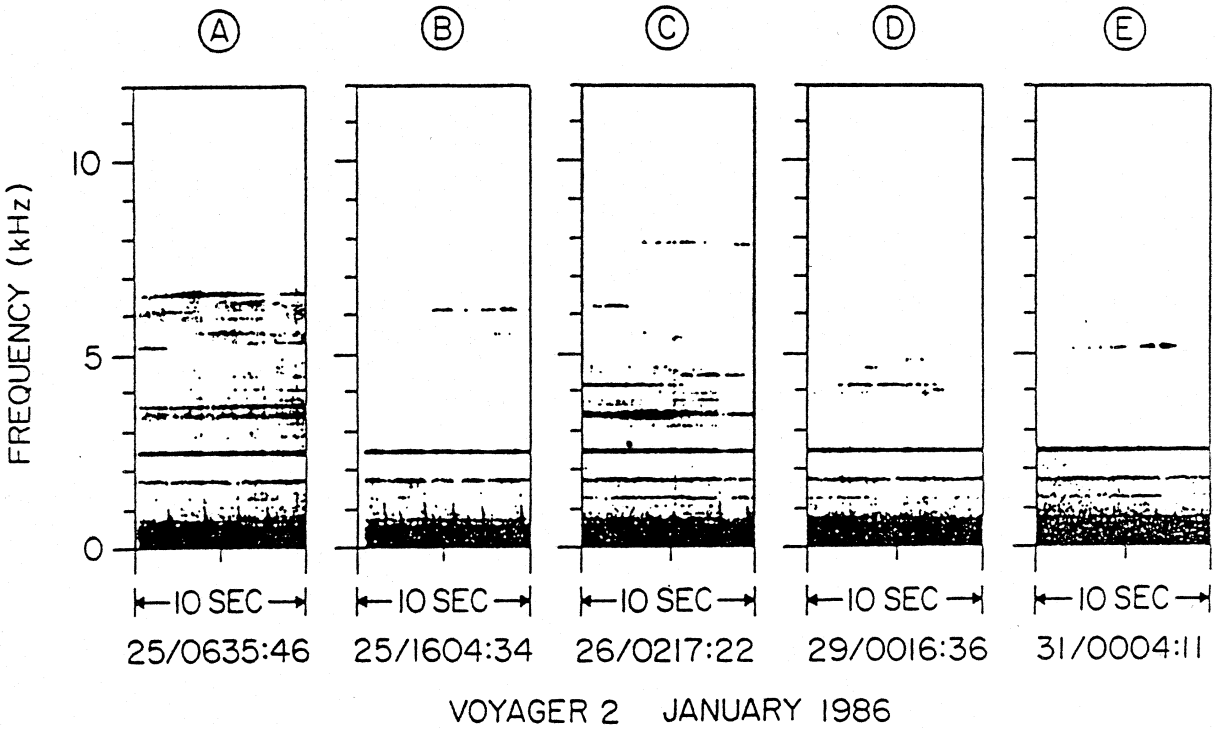

Figure 5: A series of dynamic spectra obtained from the PWS wideband experiment during periods when the narrowband radio bursts where observed. In (a) and (c), a weak diffuse background component is also observed simultaneous with the bursts. The long–lived 'streaks' in the spectrograms at 1.8 and 2.4 kHz are not bursts, but spacecraft–related interference. (Figure originally appeared in Kurth et al. [1986].)

more bursty, with intensity changes of many orders occurring on the time scales of seconds.

Figure 5, from Kurth et al. [1986], is a series of dynamic spectra obtained from the PWS wideband receiver at various times during the outbound period when the bursts were detected. It is apparent that the bursts are narrowbanded, appearing as 'streaks' across the spectrogram. The emission at a particular frequency is short–lived, persisting only for seconds (note that the 'streaks' at 1.8 and 2.4 kHz are spacecraft interference). During very active periods, such as those displayed in panel (a) and (c), a weak, diffuse background component accompanies the discrete narrowbanded bursts.

It is currently believed that the source of this emission is related to the physical processes associated at or near the Miranda L–shell [Kurth et al., 1986]. In particular, as Voyager crossed this L–shell region, very intense, narrowbanded electrostatic emissions near 9 kHz were observed by the PWS experiment. As suggested by Kurth et al. [1986], such emissions may mode convert via a linear or nonlinear process to an escaping radio emission. However, like the other bursty emissions at Uranus, the exact process creating the sporadic behavior on time scales of a second is difficult to identify.

2.6 Broadband Smooth Emission

Clearly, the most cited and discussed radio component observed at Uranus is the broadband smooth (b–smooth) emission (see Table 1). Detected in the frequency range between 150 and 900 kHz, the emission first appeared near closest approach for about 12 continuous hours [e.g., Warwick et al., 1986; Leblanc et al., 1987; Kaiser et al., 1987; Zarka and Lecacheux, 1987]. Following this first event, the emission consistently reappeared every 17 hours during the outbound period as Voyager extended to high southern magnetic latitudes; these events appearing continuous for approximately 6 to 8 hours. Since the emission was observed predominantly in the southern magnetic hemisphere, the observed emission polarization (LH) in this region is consistent with an X–mode signal. Also, the emission was one of the most powerful observed from the planet, emitting about 10^7 W. Consequently, the b–smooth component is considered one of the dominant cyclotron radio emissions from Uranus, comparable to Earth's and Saturn's auroral kilometric emissions.

Figure 1 is a color dynamic spectrum of the Voyager PRA measurements obtained during the Uranus encounter. The first b–smooth event is that occurring from 1800 SCET on 24 January to 0600 SCET on 25 January, in the frequency range between 150 and 900 kHz. Seven subsequent observations of the emission, each temporally separated by about 17 hours, are also present in the Figure. In the lower panel of the Figure, the horizontal bands seen at discrete frequencies are not natural radio signals but spacecraft–related noise. The repetition of the b–smooth event is presumably related to the rotating magnetic field system and, using a relatively large number of b–smooth occurrences, Desch et al. [1986] were able to define the planetary rotation period to better than 0.1% as 17.24 ± 0.01 hours.

As evident in Figure 1, the b–smooth emission was seen continuously during each occurrence, except at the highest frequencies (> 400 kHz) where a distinct emission intensity dropout down to the receiver noise floor was observed [Warwick et al., 1986]. These dropouts tend to occur as Voyager made its maximum excursion in southern magnetic latitude. Many investigators suggest the dropouts are a result of Voyager flying into the central region of a hollow emission cone whose apex (or source) is located near the south magnetic pole [e.g., Kaiser et al., 1987; Gulkis and Carr, 1987; Zarka and Lecacheux, 1987; Farrell and Calvert, 1989a,b]. The geometry is schematically represented in Figure 6. Assuming the radio source lies right at the magnetic pole, Barbosa [1987] inverted the observed beaming geometry to obtain a new magnetic pole position and rotation period. However, subsequent source location studies have demonstrated that the pole and source are not exactly aligned as assumed by Barbosa [1987].

Most investigators agree the b–smooth source lies relatively close to the south magnetic pole. However, results from the the source location studies differed from each other by as much as 30°. Leblanc et al. [1987] searched for the possible locations based on the emission's polarization consistent with the b–smooth observations, and derived a rather extended source whose magnetic footprint is centered at 49°S, 240°W. Lecacheux and Ortega–Molina [1987] studied the polarization reversal resulting from a spacecraft roll maneuvers, and determined that the source resides on the footprint located at 40°N, 221°W. Gulkis and Carr [1987] constructed a source located in an extended region ($\sim$

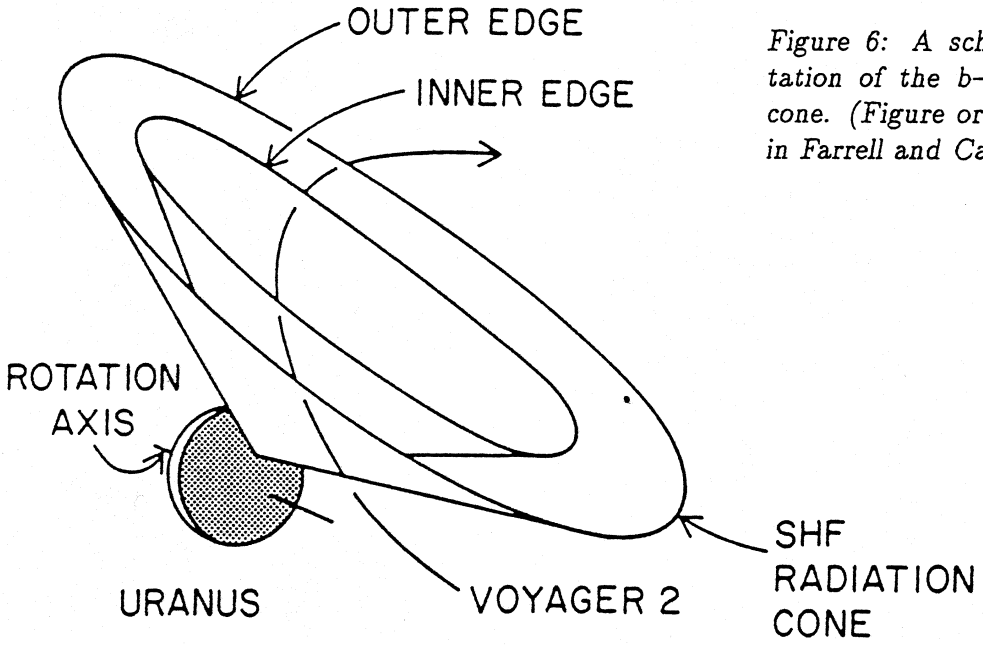

Figure 6: A schematic representation of the b–smooth emission cone. (Figure originally appeared in Farrell and Calvert, [1989b])

120° in longitude) on relatively high L–shells ($\sim$ 33) that partially surrounds the south magnetic pole, and then fit the modeled beaming geometry to the observations. In a similar approach, Romig et al. [1987] and Barbosa [1988] distributed a model source on all field lines associated with a particular L–shell, at L= 5 and 4 respectively, and again matched the beaming geometry to the observations. By careful examination of the b–smooth dropout feature, Kaiser et al. [1987] recognized that Voyager flew almost directly over the center of the radiation cone and, from this inference, derived a source footprint at 55°S, 221°W. Zarka and Lecacheux [1987] and Farrell and Calvert [1989b] fit the b–smooth observations to a radiation cone; the former comparing observations to a model emission lobe pattern and the latter fitting the edge of the dropout with a thin cone. The corresponding best–fit locations had magnetic footprints at 39°S, 216°W and 57°S, 222°W, respectively. Based on ray tracing analysis, Menietti et al. [1990] deduced that the source was very extended, occupying a 50°$\times$ 50° region centered at 50° S, 230° W. Recently, Schweitzer et al. [1990] expanded the analysis originally presented in Romig et al. [1987], and demonstrated that the source is better suited at relatively low L–shells of about 5, rather than at higher L–shell values. Figure 7, adapted from Menietti et al. [1990], shows the footprints of the b–smooth sources derived from the different investigations, including results from the most recent studies. As evident in the Figure, some of the sources lie nearly 180° apart in magnetic longitude, and thus reside on field lines that map into completely opposite magnetic hemispheres. Clearly, the different derived angular positions and source extents makes identification of the underlying physical process of the b–smooth emission very difficult.

Two theories have been presented to account for the b–smooth emission. Curtis et al. [1987] suggests that the extended atmosphere in the dayside hemisphere creates the free energy source that drives the emission. In particular, the mirror points of the radiation belt electrons in the heated and inflated sunlit hemisphere lie deeper in the atmosphere and consequently create a backscattered electron distribution with a relatively larger

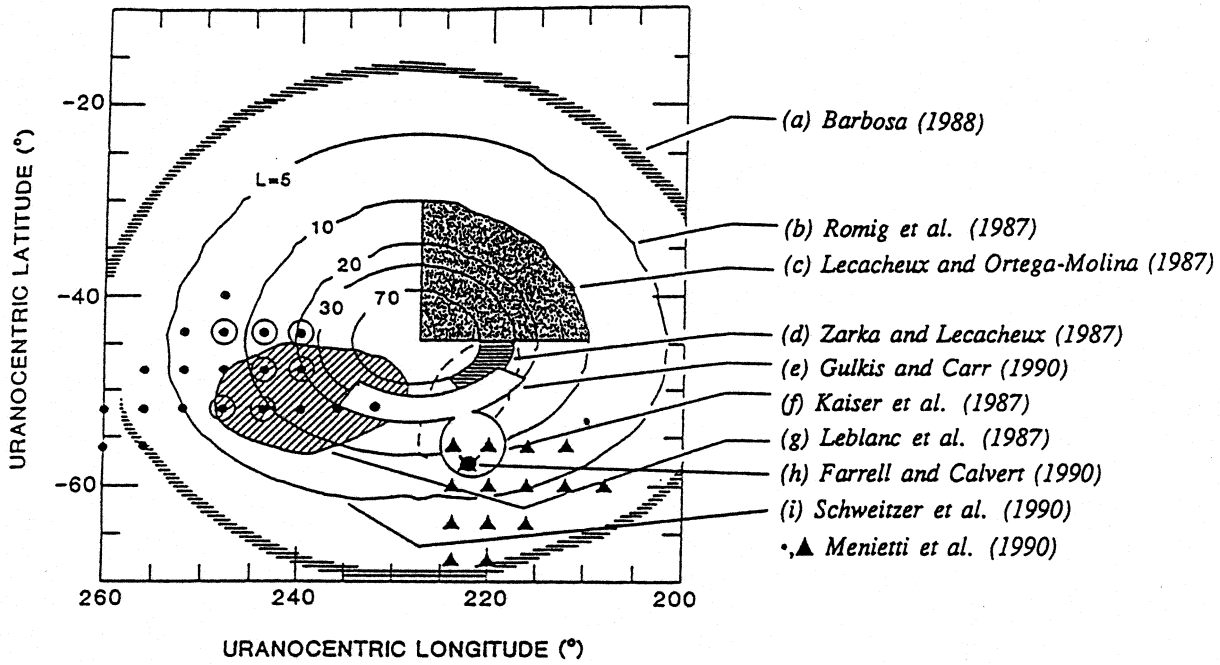

Figure 7: The proposed source locations of the b–smooth emission. Note that all suggest a southern magnetic polar source for the emission, although each very from one another by relatively large amount. (Figure adapted from Menietti et al. [1990].)

pitch angle. This unstable distribution then drives the b–smooth emission in the opposite hemisphere. In contrast, Romig et al. [1987] and Schweitzer et al. [1990], based on their source location studies, suggest that effects associated with the moon Miranda are responsible for the emission.

Warwick et al. [1987] demonstrate that the b–smooth emission is modulated at certain times during the outbound period, and suggests this results from scintillations of the emission as it propagates through density structures associated with large–scaled MHD waves on the Uranian magnetopause. Further study of these scintillations has been performed by Pedersen et al. [1992].

2.7 Broadband Bursty Emission

About an hour after Voyager crossed the magnetic equator, the PRA experiment detected a broadband bursty (b–burst) radio emission extending in frequency from about 200 kHz to 800 kHz [Warwick et al., 1986; Leblanc et al., 1987; Evans et al., 1987; Kaiser et al., 1987]. These bursty events persisted for the following four hours; each individual burst lasting on the order of 2 to 10 minutes and having very different bandwidths and center frequencies from each other. Like the b–smooth emission, episodes of the events consistently reappeared every rotation. Unlike the b–smooth emission, the bursts tended to reappear as Voyager flew near the magnetic equator. Since the emission was observed when Voyager was over the southern magnetic hemisphere, the observed polarization (LH) is consistent with the X–mode. Like the b–smooth emission, these bursts are considered

a dominant cyclotron emission [Kaiser, 1988].

Referring to Figure 1, an intense b–burst can be seen near 1500 SCET on 24 January extending from 350 to 750 kHz. Weaker events follow this one for about the next four hours. Thereafter, episodes of these bursts reappear about every 17 hours, occurring in between and out of phase with the b–smooth emission. These recurring episodes last anywhere from three to six hours.

When examined with 6–second temporal resolution, the b–burst structure appears arc–like on the scale of minutes [Calvert and Tsintikidis, 1990]. However, their appearance as a vertex–early or vertex–late arc is a function of rotational phase [see Plate 2 of Farrell and Calvert, 1989a]. When examined with 140 μsec resolution, the individual events exhibit very interesting microstructure: they consisted of periodic pulses, each lasting a few tens of milliseconds and having a repetition frequency of 30 Hz (or a period of about 30 milliseconds) [Evans et al., 1987]. This 30 Hz modulation was suspected to be related to ion density perturbations in the wave growth region [Evans et al., 1987].

Unlike the b–smooth emission, the source locations derived for the b–burst emission are in relative agreement. Evans et al. [1987] suggested a source located very near the south magnetic pole, with footprints on OTD L–shells greater than 200. Beaming from this source would be in a large hollow emission cone with an angle between 75° and 89°. Examining locations where no intrinsic polarization reversal is expected, the b–burst source footprint was derived by Leblanc et al. [1987] to be between 50°S, 233°W. By superposing the b–burst occurrences as a function of rotational phase, Farrell and Calvert [1989a] recognized that the emission extends to high frequencies twice per rotation, presumably when Voyager entered and exited the bursty radiation cone. Fitting nine of these high frequency occurrences to a magnetically field–aligned radiation cone, they deduced the source footprint to be at 48°S, 234°W, with the emission cone angles near 85°. All of these studies fall very near the b–bursty radio horizon deduced by Kaiser et al. [1987]. This horizon defines the extent of the magnetic locations within the view of the spacecraft at emission commencement and cessation (i.e., where $\vec{k} \cdot \vec{B} = 0$). For emissions beamed at or near 90° with respect to the magnetic field, the radio horizon also defines the possible source locations. As indicated in Figure 8 (which is adapted from Desch et al. [1992]), the Evans et al. [1987], Leblanc et al. [1987] and Farrell and Calvert [1989a,b] results all lie very near the Kaiser et al. [1987] radio horizon and show remarkable agreement, lying within 10° of each other. These studies suggest a source located very near the south magnetic pole, on relatively high L–shell, with emissions beamed at large angles ($\sim 80°$) with respect to the local magnetic field at the source.

One source location study differs from those presented above: The ray tracing study of Curran et al. [1990]. Using an assumed density model as an initial condition, they demonstrate that emissions initially beamed at large angles from the b–burst sources described above are highly refracted to angles near 45°. Such a beaming geometry from a single source cannot account for the emission occurrences both on the dayside (i.e., at 1515 SCET on 24 January) and on the nightside. Consequently, they suggest that there are two b–bursty sources located in opposite magnetic hemispheres, one accounting for the dayside events and the other, the nightside events. These two source locations are also shown in Figure 8.

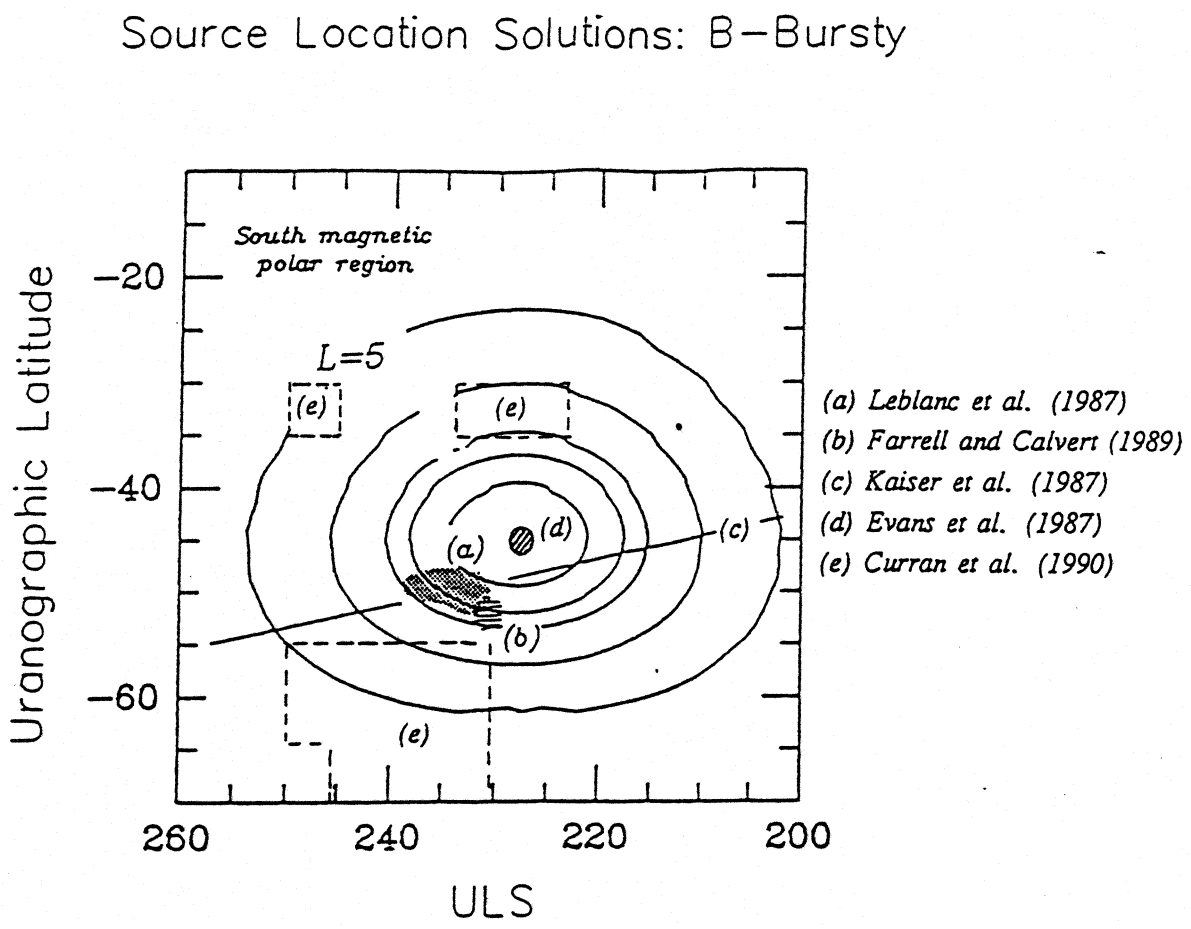

Figure 8: The proposed source locations for the b–bursty emission. (Figure adapted from Desch et al. [1992].)

The apparent discrepancy between the Curran et al. [1990] ray–tracing study and the other source location studies may have recently been accounted for by Farrell et al. [1992]. In particular, Curran et al. [1990] assumed a density model as an initial condition to the ray–tracing analysis, and then determined the final radio beaming angle. In contrast, Farrell et al. [1992] solved the converse problem: They derived the density required at the b–bursty source that can account for large beaming angles. Using an analytical cyclotron emission and ray propagation model originally presented by Calvert [1981a], they demonstrated that very low plasma densities are required in order to obtain beaming near 80°, with $n_e < 1$ cm^{-3} and $f_{pe}/f_{ce} < 0.01$. Such densities were a factor of 10^2 lower than those observed by the Radio Science (RSS) experiment at the same height in nonpolar regions [Lindal et al., 1987], thus it was concluded that the b–bursty radio source is embedded in an auroral plasma cavity, similar in structure to that associated with the Earth's auroral kilometric radio source [Calvert, 1981b]. By examination of the emission beaming geometry on a frequency–by–frequency basis, the ratio of f_{pe}/f_{ce} as a function of height was derived, and the results are illustrated in Figure 9. Consequently, an auroral plasma cavity in and around the b–bursty source can account for the beaming at large angles. Such a cavity should be included in future b–bursty ray–tracing studies.

Two theories have been presented to explain the bursty emission. Buti and Lakhina

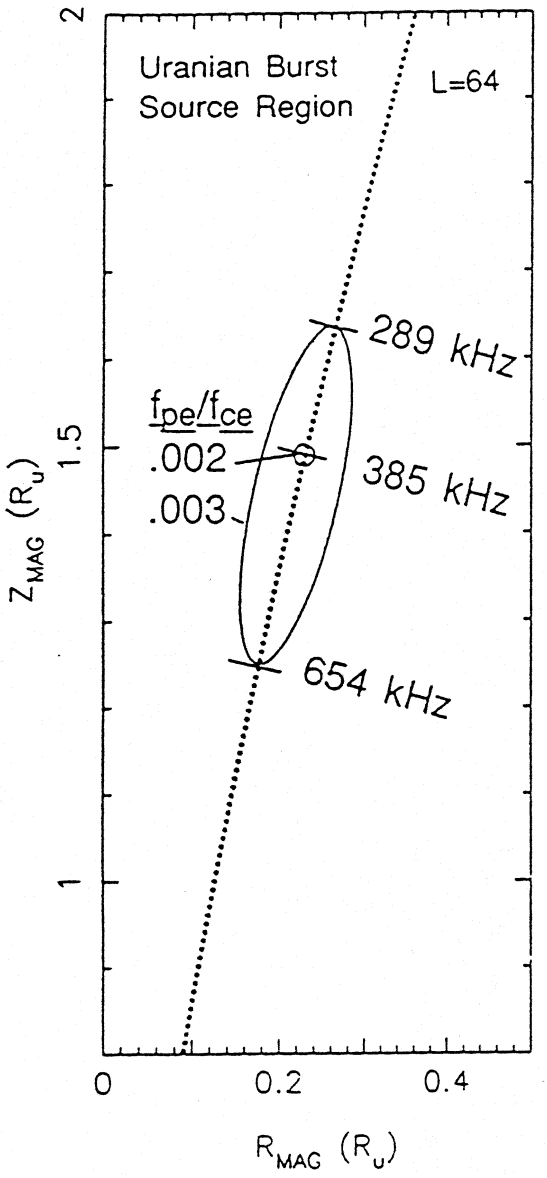

Figure 9: The ratio of f_{pe}/f_{ce} believed to be found at the b–bursty radio source region, as derived by Farrell et al. [1992]. The minimum in value along the field line suggests that the radio source is embedded within an auroral plasma cavity, much like that associated with the Earth's auroral kilometric radiation. (Figure originally appeared in Farrell et al. [1992]).

[1988] suggest the bursty character results from the nonlinear interaction between large–amplitude whistler–waves and upper hybrid waves. Wong and Goldstein [1990] suggest a beam–driven cyclotron resonance process may apply to the b–bursts.

2.8 Electrostatic Discharges

As at Saturn [Kaiser et al., 1983], the PRA experiment detected the freely–propagating radio signature of lightning–like discharges (i.e., sferics) believed to originate from the Uranian atmosphere. A comprehensive study of these emissions have been presented by Zarka and Pedersen [1986], who named these signals 'Uranian Electrostatic Discharges (UED)' , by analogy to their Saturnian counterparts [Warwick et al., 1981].

As described in Zarka and Pedersen [1986], the UEDs were detected when Voyager was within 20 R_U of the planet, in the frequency range between about 1 and 40 MHz. On a PRA spectrogram, the emission appears as a cluster of broadbanded, bursty events; each

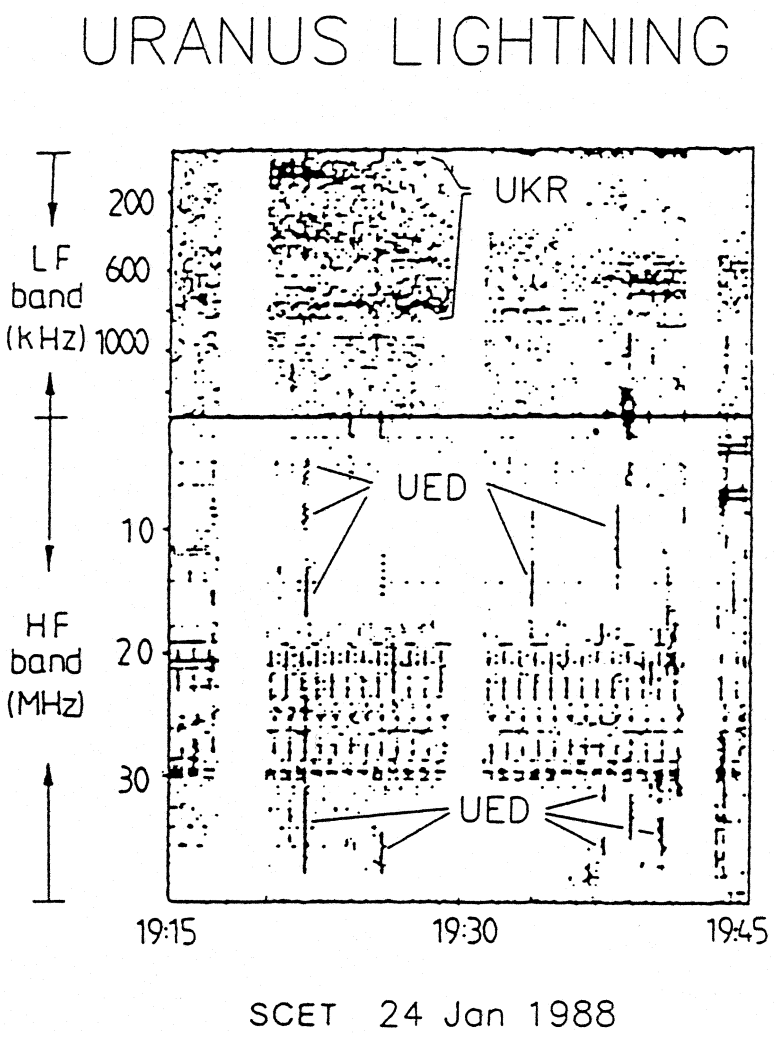

Figure 10: A PRA spectrogram contained some Uranian electrostatic discharges (UEDs). (Figure adapted from Zarka and Pedersen [1986]).

individual burst possessing a different bandwidth and center frequency. Figure 10 shows a spectrogram containing some of these events. The UED appeared in 5 or 6 separate episodes during the 24 hour period when they were observed. Unfortunately, the relatively weak emissions were not observed for long time periods like the SED's, thus the long–term periodicity (and thus their source localization in the Uranian clouds) could not be made.

The lower frequency envelop of the UED's varied, being about 7 MHz before closest approach when Voyager was over the dayside Uranian hemisphere, and dropped to near 900 kHz near closest approach, when Voyager was over the nightside hemisphere [Zarka and Pedersen, 1986]. At Saturn, the low frequency limit of the SED's was believed to be the result of the ionospheric cutoff of the radio emission at the local plasma frequency [Kaiser et al., 1983]. Assuming a similar scenario at Uranus, the UED low frequency limit of 7 MHz over the dayside hemisphere corresponds to a peak ionospheric electron density of 6×10^5 cm^{-3}, while the 900 kHz limit over the nightside corresponds to a density of 10^4 cm^{-3}. Such values are consistent with the results obtained by the Radio Science (RSS) experiment, which measured density values of 10^4–10^5 cm^{-3} near the planet's limb [Lindal et al., 1987].

The apparent bandwidth and center frequency of the UED events as seen by the PRA

receiver are affected by both the intrinsic duration of the lightning stroke and the sampling system of the PRA receiver. The PRA receiver samples from one frequency to the next every 30 msec and, consequently, any short–lived emission lasting on the order of 100's of milliseconds will be sampled in a number of adjacent frequency channels. Thus, by counting the number of channels associated with an event, an estimate of its temporal duration can be made. Using 140 UED events identified by a special computer algorithm, Zarka and Pedersen [1986] found that the typical UED event duration was about 120 msec (as compared to 60 msec for SEDs). The center frequency of each UED was random on a PRA spectrogram (like Figure 10), due to the unnatural coincidence of the event and the particular frequency being sampled.

Zarka and Pedersen [1986] also calculated the UED intensity spectrum, which is shown in Figure 11. Displayed is the averaged UED burst intensity seen at each channel, normalized to 1 AU and adjusted for the antenna/receiver response [Ortega–Molina and Daigne, 1984]. The spectrum appears to roll off at high frequencies like $1/f^2$, much like terrestrial lightning (but unlike SEDs, which possessed a flat spectrum from 0.02 to 40 MHz). The integrated power of the UED's is about 10^8 W, and is about a factor of 10 lower than that observed at Saturn. Overall, the Uranian discharges were fewer in number and weaker than those observed at Saturn.

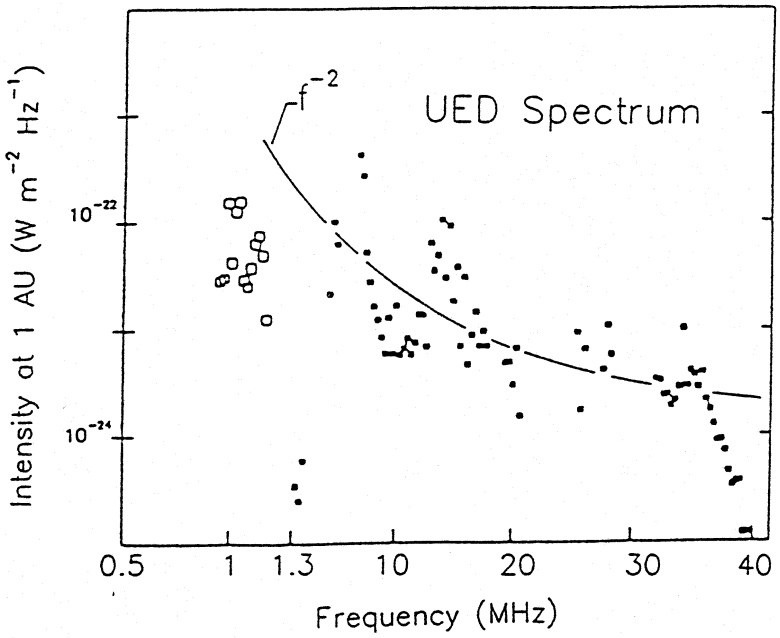

Figure 11: The UED intensity spectrum as derived by Zarka and Pedersen [1986]. Note that the emission varies in frequency approximately as $1/f^2$. (Figure adapted from Zarka and Pedersen [1986].)

2.9 Other emissions

Besides the emissions discussed above, there are other emissions that should be considered for 'componenthood'. One such emission includes a set of high frequency arc structures detected by the PRA receiver only once during the outbound period between 1100 and 1400 SCET on 25 January [Warwick et al., 1986]. These vertex–early arcs, observed between 600–800 kHz, appeared with a periodicity of about 10–min during the episode. It has been suggested [Kistler, 1988] that the arcs are driven by an Alfvénic disturbance created by the Uranian moon Ariel in a similar way as the Io–related Jovian decametric component [Gurnett and Goertz, 1981]. Another emission considered for 'componenthood' is a vertex–early arc emission detected between about 200–400 kHz seen in association with about half of the b–smooth occurrences [Farrell and Calvert, 1990]. The source of this emission was found to lie very near that of the b–smooth location, suggesting a common free energy source. Grabbe [1988a,b] suggested that an emission observed by the PWS wideband experiment may result from the spacecraft intercepting X–mode resonance cones.

3 Uranus as a radio source: General properties

As evident in the previous section, there has been much work on localizing the various radio sources at Uranus. The value of such studies is that they identify magnetospherically–active regions at the planet. On a spinning spacecraft, source localization can be made directly as the antennas align themselves with the radiated electric field emitted from a radio source. Since Voyager is not a spinning spacecraft, the source localization process is model–dependent, and therefore somewhat less direct. Despite this drawback, one can consider that we are 'viewing' these active source regions in the hectometric and kilometric radio regime (albeit indirectly), and these radio 'images' of the active source regions can be compared to those made at sub–millimeter wavelength (i.e., UV observations). Figure 12 is a very powerful presentation, combining results from the PRA, UVS and MAG experiments. Shown in the Figure is a preliminary map of the UV intensity near the planet cloud tops between 875 and 1100 Angstroms obtained from the UVS measurements using the general inverse approach with a spherical harmonic basis [Herbert and Sandel, 1990]. In the Figure, UV intensities are represented by grayshading and light contours. Superimposed on the Figure, in dark contours, are the magnetic L–shells at the cloud tops derived from the Q3 magnetic field model [Connerney et al., 1987]. Finally, the radio source locations of the auroral–type emissions (i.e., the n–bursty, O–mode, b–bursty, and b–smooth emissions) are indicated on the Figure. The radio source regions shown are not from any individual study, but represent the region where most of the derived locations for a particular emission can be found. The extended region associated with the b–smooth emission contains nearly all the locations shown in Figure 7. The region associated with the b–bursts contains the (a), (b) and (d) shown in Figure 8. The n–burst source was that obtained from Farrell et al. [1990a] and the O–mode source was that from Desch and Kaiser [1987] (which is a subsection of the Menietti and Curran [1990b] source).

Consider the south magnetic polar region first. It is evident that the UV hot spot in this

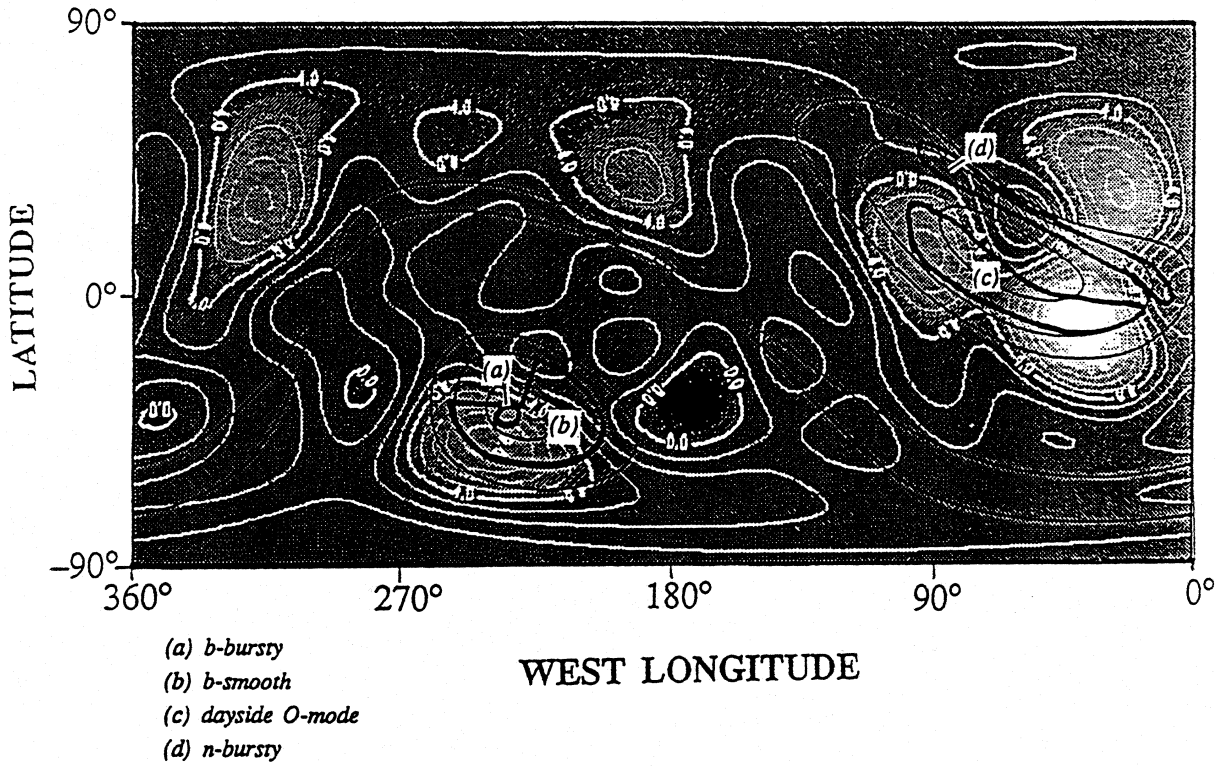

Figure 12: Shown is the UV intensity between 800–1100 Angstroms near the cloud top, as derived by the generalized inverse method applied by Herbert and Sandel [1990], the Q3 model [Connerney et al., 1987] magnetic L–shells for values of L=1, 3, 5 and 20, and the source positions of the auroral radio emissions (i.e., the b–smooth, b–bursty, n–smooth and n–bursty emissions).

region does not coincide exactly with the Q3 south pole position, but is in fact located approximately 15° to the southwest of the pole. It is most interesting to note that the position of this auroral hot spot lies just south of the b–burst radio source position. From this comparison, it appears that the b–bursty source lies at the northern edge of the auroral hot spot, while the rather extended b–smooth source location contains the entire hot spot. Thus, near the south magnetic pole, the association of the radio and UV hot spots seems particularly good. Consider now the northern magnetic polar region. As indicated in Figure 12, there is a very complicated UV signature associated with this pole, with a number of hot regions surrounding the region of large L–shell value. Unfortunately, the n–burst source does not coincide with any one of these spots. The situation is better for the dayside O–mode source, which seems to envelop a hot spot south of the north magnetic pole. This association suggests that the UV active region is the source of the emission. Although the association of radio and UV hot spots near the north pole is not extremely convincing, the observations certainly suggest that this pole, in general, is active.

Figure 13, from Desch et al. [1992], shows the median radio flux density spectra for Earth, Jupiter, Saturn, and Uranus' nightside emissions, all normalized to 1 AU. The radio power from Neptune, not included in the Figure, is slightly less than that observed at Uranus [Warwick et al., 1987]. Based on these spectra, the total frequency–intergrated median

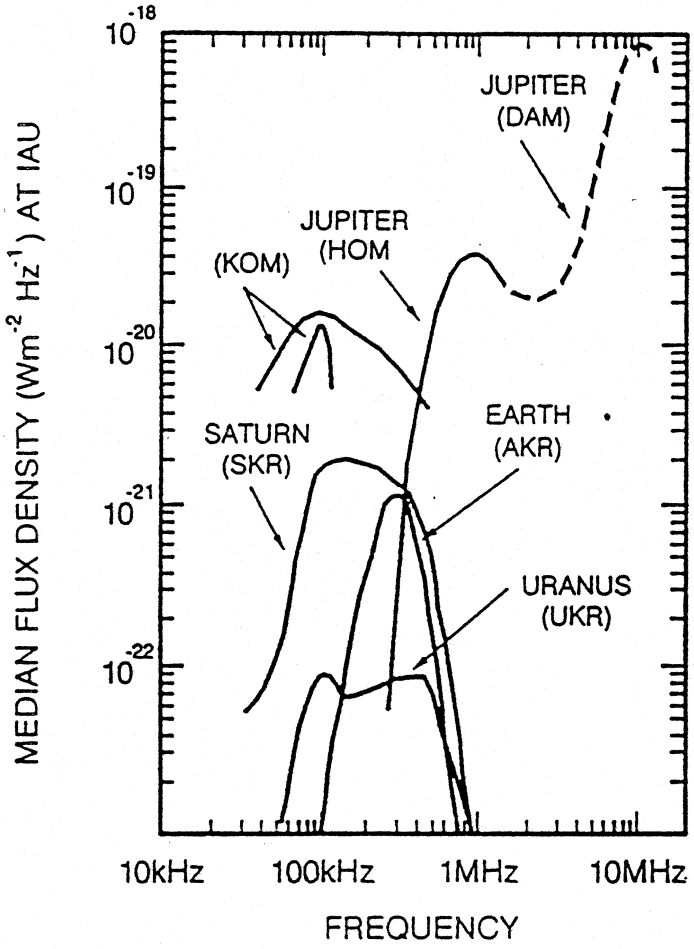

Figure 13: The median radio flux density at Jupiter, Saturn, Earth and Uranus. (Figure originally appeared in Desch et al. [1992]).

power from Uranus' nightside south magnetic polar region was calculated to be about 10^7 W. In contrast, the median power associated with the n–bursts created from the dayside north magnetic pole is approximately 10^6 W [Desch et al., 1992], which is about a factor of 10 lower than the nightside generated emissions. The power of the dayside O–mode emission, also generated from the north magnetic pole, is weaker still, being about 5×10^5 W [Desch and Kaiser, 1987]. Because of the relatively low power the dayside generated emissions, Uranus defied the discovery prediction based upon the radiometric Bodes law [Desch and Kaiser, 1984]. However, the much higher radiated power from the nightside pole is consistent with this law and suggests that the ultimate driver of the Uranian emissions is the solar wind [Desch et al., 1992]. The failure of the radiometric Bodes law in predicting the correct discovery time lies in the fact that it does not include beaming effects [Desch and Kaiser, 1984], which were critical at Uranus. Consequently, Curtis' [1985] nightside beaming prediction was, in essence, true.

As discussed in Desch et al. [1992], the radio planets can be classified into two categories: Those with complex emission morphologies and those with relatively simple morphologies. Clearly, Earth and Saturn fall in the latter category of simplicity. Both possess one strong auroral kilometric radio emission and a single equator continuum–type emission. In contrast, Jupiter, Uranus, and Neptune possess very complex morphologies. Each of these planets had multiple components consisting of both very smooth and very burst emission

types. Jupiter appears to be a study of complexity unto itself, possessing both Io and non–Io driven components. A superficial examination suggests that Uranus and Neptune have similar radio morphologies, each possessing a dominant smooth and a dominant bursty radio type [Warwick et al., 1986; Warwick et al., 1987]. However, when examined closely, there are subtle differences. For example, all totaled, Uranus possess three bursty components, while Neptune, to date, possess two components [Farrell et al., 1990b; Desch et al., 1991]. Also, the dominant emissions at Neptune were not preferentially beamed, like at Uranus.

4 Conclusions

Through mid–1991, there were approximately 48 investigative studies of the various Uranian radio components. Figure 14 shows the number of papers produced as a function of time. In 1987, a maximum of twelve papers were produced, as might be expected a year following the encounter. However, three years later, twelve papers were again published. This second peak in the distribution is believed to result from the numerous studies published under the auspices of NASA's Uranus Data Analysis Program (UDAP). Out of the total of 48 papers, 5 were predictions, 11 dealt with initial observations, 19 cover source locations, 9.5 discussed theory, and 4.5 were reviews. One can conclude that PRA and PWS investigators were very productive, given that the respective data sets contain only about two weeks of significant information from Uranus.

From the investigations, numerous new discoveries were made. The PRA and PWS radio teams were the first to substantiate that Uranus possessed a significant magnetic field [Gurnett at al., 1986]. They also calculated the planetary rotation period to better than 0.1% [Desch et al., 1986], and determined that both north and south magnetic polar regions, along with the equator region, are magnetospherically–active. Inspired by the Uranus observations, numerous theories of wave/particle and wave/wave interactions were developed to fit the observations, including a nonlinear electrostatic to EM wave conversion theory [Buti and Lakhina, 1988], a surface MHD wave to EM wave conversion theory [Farrell et al., 1992], a beam–driven cyclotron resonance theory [Wong and Goldstein, 1990], and a terminator–driven electromagnetic wave theory [Curtis et al., 1987]. As a consequence of the encounter, many interesting advances have been made in both radio wave observation and theory.

In the distant future, questions about the radio emission properties might be addressed by a Uranus Orbiter. Unfortunately, given the current financial and political climate, the development of such an orbiter is highly speculative. However, in the near future, observations of Uranian radio emissions obtained from inner–solar system probes, like Ulysses, may be made in the mid–to–late 1990's as the sub–spacecraft position at Uranus intersects the magnetic equator, which is the region favorable for b–bursts observations [Kaiser, 1988].

It should be recognized that the Voyager flyby in 1986 resulted in a determination of the radio morphology at Uranus at a specific orbital phase, when the planet's rotational pole was pointing sunward and the north magetic pole was sunlit. The radio morphology

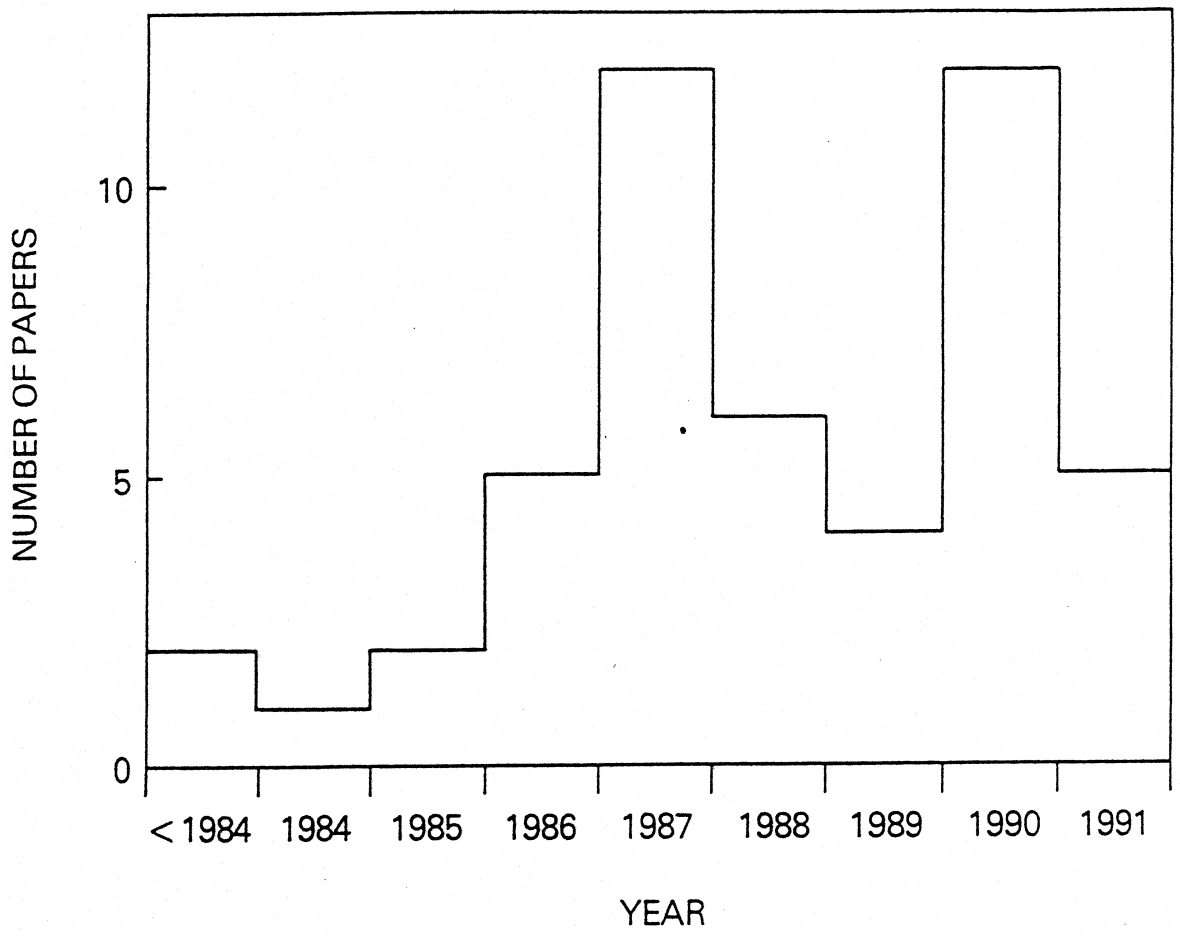

Figure 14: The number of paper investigating the Uranian radio emissions as a function of time.

may be very different in 2028, 42 years after the encounter, when the rotational pole is antisunward and the south pole is sunlit. In this new case, the dominant emissions near the strong, south magnetic pole may reduce in intensity or disappear altogether, since they are no longer connected to a nightside energy source. Such variations of the radio morphology with orbital phase are not expected from the other radio planets, only from Uranus with its very unusual orientation of the rotation and magnetic poles.

Acknowledgments: I would like to thank F. Herbert for supplying the UV intensity map shown in Figure 12.

References

Barbosa, D. D., Beaming of Uranian kilometric radiation and implications for the planetary magnetic field, *Astrophys. J.*, **315**, L151–L154, 1987.

Barbosa, D. D., Polar cap emission model of Uranian kilometric radiation, *Astrophys. J.*, **333**, 443–451, 1988.

Brown, L. W., Possible radio emission from Uranus at 0.5 MHz, *Astrophys. J.*, **207**, L209–L212, 1976.

Buti, B., and G. S. Lakina, Source of bursty radio emissions from Uranus, *Geophys. Res. Lett.*, **15**, 1149–1152, 1988.

Calvert, W., A theory for the auroral kilometric and Jovian decametric radiation cones, *Univ. of Iowa Res. Rept.*, 81–6, 1981a.

Calvert, W., The auroral plasma cavity, *Geophys. Res. Lett.*, **8**, 919–921, 1981b.

Calvert, W., and D. Tsintikidis, New Voyager radio spectrograms of Uranus, *Univ. of Iowa Res. Rept.*, 90–13, 1990.

Clarke, J. T., Detection of auroral H Ly–α emission from Uranus, *Astrophys. J. Lett.*, **263**, L105–L109, 1982.

Connerney, J. E. P., M. H. Acuña, and N. F. Ness, The magnetic field of Uranus, *J. Geophys. Res.*, **92**, 15329–15336, 1987.

Curran, D. B., and J. D. Menietti, Narrowbanded bursty radio emissions at Uranus (abstract), *AGU EOS Trans.*, **71**, 597, 1990.

Curran, D. B., J. D. Menietti, and H. K. Wong, Ray tracing of brodband bursty radio emissions from Uranus, *Geophys. Res. Lett.*, **17**, 109–112, 1990.

Curtis, S. A., Possible nightside source dominance in nonthermal radio emissions from Uranus, *Nature*, **318**, 47–48, 1985.

Curtis, S. A., M. D. Desch, and M. L. Kaiser, The radiation belt origin of Uranus' nightside radio emission, *J. Geophys. Res.*, **92**, 15199–15205, 1987.

Desch, M. D., and H. O. Rucker, The relationship between Saturn kilometric radiation and the solar wind, *J. Geophys. Res.*, **88**, 8999–9006, 1983.

Desch, M. D., and C. H. Barrow, Direct evidence for solar wind control of Jupiter's hectometer–wavelength radio emission, *J. Geophys. Res.*, **89**, 6819–6823, 1984.

Desch, M. D., and M. L. Kaiser, Predictions for Uranus from a radiometric Bode's law, *Nature*, **310**, 755–757, 1984.

Desch, M. D., J. E. P. Connerney, and M. L. Kaiser, The rotation period of Uranus, *Nature*, **322**, 42–43, 1986.

Desch, M. D., and M. L. Kaiser, Ordinary mode radio emission from Uranus, *J. Geophys. Res.*, **92**, 15211–15216, 1987.

Desch, M. D., M. L. Kaiser, and W. S. Kurth, Impulsive solar wind–driven emission from Uranus, *J. Geophys. Res.*, **94**, 5255–5263, 1989.

Desch, M. D., W. M. Farrell, and M. L. Kaiser, An anomalous component of Neptune radio emission: Implications for the auroral zone, *J. Geophys. Res.*, **96**, 1401–1408, 1991.

Desch, M. D., M. L. Kaiser, P. Zarka, A. Lecacheux, Y. Leblanc, M. Aubier, and A. Ortega–Molina, Uranus as a radio source, To appear in *Uranus*, Univ. of Arizona Press, 1992.

Evans, D. R., J. H. Romig, and J. W. Warwick, Bursty radio emissions from Uranus, *J. Geophys. Res.*, **92**, 15206–15210, 1987.

Farrell, W. M., and W. Calvert, The source location and beaming of brodband bursty radio emissions from Uranus, *J. Geophys. Res.*, **94**, 217–225, 1989a.

Farrell, W. M., and W. Calvert, Source location of the smooth high–frequency radio emissions from Uranus, *Geophys. Res. Lett.*, **16**, 341–344, 1989b.

Farrell, W. M., and W. Calvert, New arcs associated with the smooth high frequency radiation at Uranus, *J. Geophys. Res.*, **95**, 8259–8264, 1990.

Farrell, W. M., M. D. Desch, M. L. Kaiser, and W. S. Kurth, Source location of the narrowbanded radio bursts at Uranus: Evidence of a cusp source, *Geophys. Res. Lett.*, **17**, 295–298, 1990a.

Farrell, W. M., M. D. Desch, and M. L. Kaiser, Field–independent source localization of Neptune's radio bursts, *J. Geophys. Res.*, **95**, 19143–19148, 1990b.

Farrell, W. M., M. D. Desch, M. L. Kaiser, and W. Calvert, Evidence of auroral plasma cavities at Uranus and Neptune from radio burst observations, *J. Geophys. Res.*, **96**, 19049, 1991.

Farrell, W. M., S. A. Curtis, M. D. Desch, and R. P. Lepping, A theory for narrowbanded radio bursts at Uranus: MHD surface waves as an energy driver, *J. Geophys. Res.*, **97**, 4133, 1992.

Grabbe, C., Extraordinary–mode resonance cones in the Uranian magnetosphere?, *J. Geophys. Res.*, **93**, 14304–14315, 1988a.

Grabbe, C., Extraordinary–mode waves on the resonance cone detected at Uranus, in *Planetary Radio Emissions II*, edited by H. O. Rucker, S. J. Bauer, and B. M. Pedersen, Austrian Academy of Sciences Press, Vienna, 1988b.

Gulkis, S., and T. D. Carr, The main source of radio emission from the magnetosphere of Uranus, *J. Geophys. Res.*, **92**, 15159–15168, 1987.

Gurnett, D. A., and C. K. Goertz, Multiple Alfvén wave reflections excited by Io: Origins of the Jovian decametric arcs, *J. Geophys. Res.*, **86**, 717–722, 1981.

Gurnett, D. A., W. S. Kurth, F. L. Scarf, and R. L. Poynter, First plasma wave observations at Uranus, *Science*, **233**, 106–109, 1986.

Herbert, F., and B. R. Sandel, The Uranian aurora. The Magnetospheres of the Outer Planets, Fred Scarf Symposium, August 20–24, Annapolis, MD, 1990.

Hill, T. W., and A. J. Dessler, Remote sensing of the magnetic moment of Uranus: Prediction for Voyager, *Science*, **227**, 1460–1469, 1985.

Jones, D., Source of terrestrial non–thermal radiation, *Nature*, **260**, 686–689, 1976.

Jones D., Latitudinal beaming of planetary radio emissions, *Nature*, **288**, 225–229, 1980.

Kaiser, M. L., J. E. P. Connerney, and M. D. Desch, Atmospheric storm explanation of Saturn's electrostatic discharges, *Nature*, **303**, 50–53, 1983.

Kaiser, M. L., M. D. Desch, and S. A. Curtis, The sources of Uranus' dominant nightside radio emissions, *J. Geophys. Res.*, **92**, 15169–15176, 1987.

Kaiser, M. L., Uranus radio emissions, in *Planetary Radio Emissions II*, edited by H. O. Rucker, S. J. Bauer, and B. M. Pedersen, Austrian Academy of Sciences Press, Vienna, 1988.

Kaiser, M. L., M. D. Desch, and J. E. P. Connerney, Radio emission from the magnetic equator of Uranus, *J. Geophys. Res.*, **94**, 2399–2404, 1989.

Kennel, C. F., and J. E. Maggs, Possibility of detecting magnetospheric radio bursts from Uranus and Neptune, *Nature*, **261**, 299–301, 1976.

Kistler, A. C., Voyager 2 detection of Uranian hectometric radio arcs, M.S. Thesis, University of Iowa, 1988.

Kurth, W. S., D. A. Gurnett, and F. L. Scarf, Sporadic narrowband radio emissions from Uranus, *J. Geophys. Res.*, **91**, 11959–11964, 1986.

Kurth, W. S., D. A. Gurnett, and M. D. Desch, Continuum radiation at Uranus, *J. Geophys. Res.*, **95**, 1103–1111, 1990.

Lecacheux, A., and A. Ortega–Molina, Polarization and localization of the Uranian radio sources, *J. Geophys. Res.*, **92**, 15148–15158, 1987.

Leblanc, Y., M. G. Aubier, A. Ortega–Molina, and A. Lecacheux, Overview of the Uranian radio emission: Polarization and constraints on source locations, *J. Geophys. Res.*, **92**, 15125–15138, 1987.

Lindal, G. F., J. R. Lyons, D. N. Sweetnam, V. R. Eshleman, D. P. Hinson, and G. L. Tyler, The atmosphere of Uranus: Results of radio occultation measurements with Voyager 2, *J. Geophys. Res.*, **92**, 14987–15001, 1987.

Menietti, J. D., H. K. Wong, D. A. Wah, and C. S. Lin, Source region of the smooth high–frequency nightside Uranus kilometric radiation: A ray–tracing study, *J. Geophys. Res.*, **95**, 51–60, 1990.

Menietti, J. D., and D. B. Curran, Possible second harmonic gyroemission at Uranus, *J. Geophys. Res.*, **95**, 20959–20966, 1990a.

Menietti, J. D., and D. B. Curran, Source of O–mode radio emissions from the dayside of Uranus, *J. Geophys. Res.*, **95**, 15263–15267, 1990b.

Ness, N. F., M. H. Acuña, K. W. Behannon, L. F. Burlaga, J. E. P. Connerney, R. P. Lepping, and F. M. Neubauer, Magnetic fields at Uranus, *Science*, **233**, 85–89, 1986.

Ortega–Molina, A., and G. Daigne, Polarization response of two crossed monopoles on a spacecraft, *Astron. Astrophys.*, **130**, 301–310, 1984.

Pedersen, B. M., M. G. Aubier, and M. D. Desch, Scintillations of the Uranian kilometric radiation: Implications for the downstream magnetopause, *J. Geophys. Res.*, **97**, 8127, 1992.

Rabl, G. K. F., H. P. Ladreiter, H. O. Rucker, and Y. Leblanc, Uranus smooth low frequency emissions, *Annales Geophys.*, **9**, 487–494, 1991.

Rabl, G. K. F., H. P. Ladreiter, H. O. Rucker, and Y. Leblanc, Uranus smooth low frequency emissions, *Adv. Space Res.*, **12**, (8)117–(8)120, 1992.

Romig, J. H., D. R. Evans, C. B. Sawyer, A. E. Schweitzer, and J. W. Warwick, Models of Uranian continuum radio emission, *J. Geophys. Res.*, **92**, 15189–15198, 1987.

Sawyer, C., K. L. Neal, and J. W. Warwick, Polarization model applied to Uranian radio emission, *J. Geophys. Res.*, **96**, 5575, 1991.

Scarf, F. L., and D. A. Gurnett, A plasma wave investigation for the Voyager mission, *Space Sci. Rev.*, **21**, 289–308, 1977.

Schweitzer, A. E., J. H. Romig, D. R. Evans. C. B. Sawyer, and J. W. Warwick, Offset, tilted dipole models of Uranian smooth high–frequency radio emission, *J. Geophys. Res.*, **95**, 14977–14986, 1990.

Warwick, J. W., J. B. Pearce, R. G. Peltzer, and A. C. Riddle, Planetary Radio Astronomy experiment for Voyager missions, *Space Sci. Rev.*, **21**, 309–319, 1977.

Warwick, J. W., J. B. Pearce, D. R. Evans, T. D. Carr, J. J. Schauble, J. K. Alexander, M. L. Kaiser, M. D. Desch, B. M. Pedersen, A. Lecacheux, G. Daigne, A. Boischot, and C. H. Barrow, Planetary Radio Astronomy observations from Voyager 1 near Saturn, *Science*, **212**, 239–243, 1981.

Warwick, J. W., D. R. Evans, J. H. Romig, C. B. Sawyer, M. D. Desch, M. L. Kaiser, J. K. Alexander, T. D. Carr, D. H. Staelin, S. Gulkis, R. L. Poynter, M. Aubier, A. Boischot, Y. Leblanc, A. Lecacheux, B. M. Pedersen, and P. Zarka, Voyager 2 radio observations of Uranus, *Science*, **233**, 102–106, 1986.

Warwick, J. W., D. R. Evans, and P. B. Dusenbery, Waves on the Uranian downstream magnetopause, *J. Geophys. Res.*, **92**, 15367–15375, 1987.

Warwick, J. W., D. R. Evans, R. G. Peltzer, J. H. Romig, C. B. Sawyer, A. C. Riddle, A. E. Schweitzer, M. D. Desch, M. L. Kaiser, W. M. Farrell, T. D. Carr, I. de Pater, D. H. Staelin, S. Gulkis, R. L. Poynter, A. Boischot, F. Genova, Y. Leblanc, A. Lecacheux, B. M. Pedersen, P. Zarka, Voyager planetary radio astronomy at Neptune, *Science*, **246**, 1498–1501, 1989.

Wu, C. S., and L. C. Lee, A theory of the terrestrial kilometric radiation, *Astrophys. J.*, **230**, 621–626, 1979.

Wong, H. K., and M. L. Goldstein, A mechanism for bursty radio emissions in planetary magnetospheres, *Geophys. Res. Lett.*, **17**, 2229–2232, 1990.

Zarka, P., and F. Genova, Low–frequency Jovian emission and solar wind magnetic sector structure, *Nature*, **306**, 767–768, 1983.

Zarka, P., and B. M. Pedersen, Radio detection of Uranian lightning by Voyager 2, *Nature*, **323**, 605–608, 1986.

Zarka, P., and A. Lecacheux, Beaming of Uranian nightside kilometric radio emission and inferred source location, *J. Geophys. Res.*, **92**, 15177–15188, 1987.